General relationships between the mobility of a chain fluid and various computed scalar metrics

Joanne Budzien, John D. McCoy, and Douglas B. Adolf

Citation: The Journal of Chemical Physics **121**, 10291 (2004); doi: 10.1063/1.1808694
View online: http://dx.doi.org/10.1063/1.1808694
View Table of Contents: http://scitation.aip.org/content/aip/journal/jcp/121/20?ver=pdfcov
Published by the AIP Publishing

General relationships between the mobility of a chain fluid and various computed scalar metrics

Joanne Budzien and John D. McCoy
New Mexico Institute of Mining and Technology, Socorro, New Mexico 87801

Douglas B. Adolf
Sandia National Laboratories, Albuquerque, New Mexico 87185-0888

(Received 16 June 2004; accepted 30 August 2004)

We performed molecular dynamics simulations of chain systems to investigate general relationships between the system mobility and computed scalar quantities. Three quantities were found that had a simple one-to-one relationship with mobility: packing fraction, potential energy density, and the value of the static structure factor at the first peak. The chain center-of-mass mobility as a function of these three quantities could be described equally well by either a Vogel-Fulcher type or a power law equation. © *2004 American Institute of Physics.* [DOI: 10.1063/1.1808694]

I. INTRODUCTION

Structural glasses display a dramatic increase of relaxation times with decrease of temperature. The kinetic glass transition is the direct result of this. When the relaxation time exceeds the time scale of the experiment, the system falls out of equilibrium. This is evidenced in changes in the coefficient of thermal expansion and jumps in heat capacity.

Not surprisingly, the kinetic glass transition is rate dependent. Cooling more slowly allows the system to equilibrate and the transition shifts to lower temperatures. However, in many systems, the relaxation time increases so rapidly with decreasing temperature that it extrapolates to infinity at a finite temperature $\tilde{T}$. In such cases, the time scale of the experiment would not matter, the system could not possibly equilibrate for temperatures less than $\tilde{T}$. Whether this $\tilde{T}$ is evidence of an underlying, ideal glass transition or is simply an artifact of the extrapolation procedure is a point of much controversy.

Be that as it may, the infinite relaxation time limit is still useful, even if the nature of $\tilde{T}$ is not fully understood. There are two prevalent expressions relating the relaxation time τ to temperature that incorporate a divergence in the relaxation time. One is the Vogel-Fulcher (VF) equation

$$\ln(\tau) = A + \frac{B}{T - T_0}, \tag{1}$$

where T is the temperature and A, B, and T_0 are constants with respect to temperature. The other is a power-law form taken from critical point phenomena,

$$\tau \propto (T - T_C)^{-\gamma}, \tag{2}$$

where T_c and the exponent γ are constants. In cases where the two functional forms have been compared, it appears that a similar range of temperatures is fit in both equations.[1,2] However, the two equations generally predict different points of divergence (i.e., T_C is not equal to T_0).

A severe limitation of these representations lies in the fact that the parameters are strongly path dependent; that is, they vary depending upon the exact pressure-volume-temperature path chosen for the experimental study. This limitation is examined in Fig. 1(a), where the mobilities (defined as diffusion coefficient D divided by temperature) from a series of simulations are presented in a traditional Arrhenius plot, D/T vs $1/T$. Note that the mobility is effectively an inverse relaxation time. Two types of systems are considered: ''attractive'' systems with Lennard-Jones nonbonded interactions, and ''repulsive'' systems with only the repulsive inner wall of the Lennard-Jones potential. More importantly, the simulation series follow two distinct types of thermodynamic paths, isochoric or isobaric. Clearly, the mobility is not a function of temperature alone; it depends on path and system type. Moreover, some curves appear Arrhenius while some must be fit with Eqs. (1) or (2) so even the shape of the curves is path dependent.

In the current study, we want to correlate mobility with system properties for two purposes. First, we want to develop an extrapolation tool that is path independent (although, perhaps, still system dependent). Second, we want to examine the factors that affect mobility with the eventual goal of understanding causes of the glass transition. We do this without a mechanistic model for mobility; at this stage of investigation, we seek correlation, not causation.

We use the term ''scalar metric'' to identify thermostatic system properties that can be used to correlate mobility in a one-to-one manner (i.e., collapse all data to a single ''master curve'') and can be described using relations incorporating a divergence in mobility. A benefit of correlating mobility with system properties in a master curve manner is the ease of defining ''distance'' to the transition since there is now only a single relevant parameter.

The idea of correlating the mobility of a system with system properties is not new especially as applied to determining causes of the glass transition. Traditionally, in a thermostatic worldview, one considers correlating mobility with free volume[3–5] or configurational entropy.[6] In the literature, dynamic properties have been considered as well, most notably through mode-coupling theory[7] and facilitated

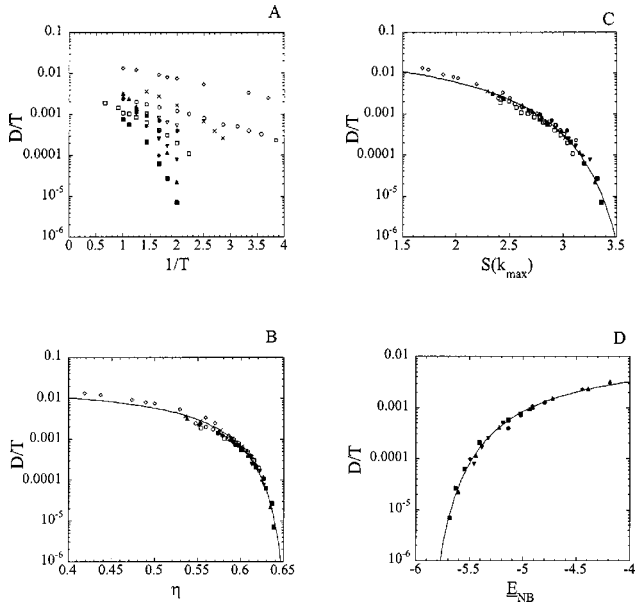

FIG. 1. This figure shows the chain center-of-mass mobility (D/T) as a function of four quantities. The data are the same in each part of the figure, only the abscissa variable has changed. Lines are best fits from Eq. (11). (a) D/T vs $1/T$ for a few thermodynamic cooling paths. Circles are $\rho=1.00$, down triangles are $\rho=1.033$, squares are $\rho=1.06$, and diamonds are $P=3.2$. Filled symbols are attractive systems; open symbols are repulsive systems. Filled up triangles are $P=2.0$ for an attractive system, *x*'s are $P=6.5$ for a repulsive system. (b) D/T vs η (c) D/T vs $S(k_{\max})$ (d) D/T vs $\underline{E}_{\mathrm{NB}}$.

dynamics.[8] We choose here to focus on static properties that are readily available from simulation. The purpose of this, again, stems from the absence of a mobility mechanism; we use quantities as scalar metrics that are already well defined and do not postulate any new theoretical parameters. We focus on thermostatic properties due to the idea that forces, temperature, and structure should lead to dynamics.

As can be seen in Fig. 1(a), temperature alone is not the appropriate scalar quantity to collapse all data. Discussions in the recent literature have debated whether temperature or density effects dominate glass transition behavior.[9] The conclusion seems to be strongly system dependent;[10,11] yet, the mobility empirically seems to follow the relationship[12]

$$\ln\left(\frac{D}{T}\right)\propto T^{-1}V^{-C}, \tag{3}$$

where V is specific volume and C is a material dependent constant that increases as density effects increase. We fit our data using this relation in Fig. 2. Both attractive (with $C=8.0$) and repulsive systems (with $C=12$) collapse to single system-dependent curves. As one would expect, density is more dominant in the repulsive systems. This method may be valid as an extrapolation tool (our first purpose of this study), but it is less clear how this relates to finding factors that cause the glass transition (the second purpose of this study).

In our approach, temperature and density are not assumed fundamental properties [as was done in Eq. (3)]. Rather, we have investigated several scalar metrics that naturally incorporate the pressure-volume-temperature (P-V-T) response.[13] Collapse of the mobility data when plotted against these metrics [as seen in Figs. 1(b), 1(c), and 1(d)] suggests that they correctly capture these correlated responses.

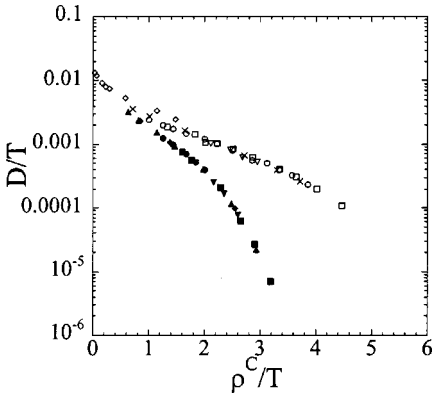

FIG. 2. The data collapse using Eq. (3). Symbols are the same as in Fig. 1. Attractive systems, $C=8.0$. Repulsive systems, $C=12.0$.

In this study, simulations of short, bead-spring, chain molecules at different temperatures and pressures were performed for two different intermolecular potential types: a cut-and-shifted Lennard-Jones 12-6 interaction that includes attractions and a cut-and-shifted Lennard-Jones 12-6 potential that is fully repulsive. The diffusion coefficients for the chain centers of mass were determined and used as measures of system mobility D/T. We found three scalar metrics that correlated all mobility data regardless of thermodynamic path: (1) the packing fraction η, (2) the first peak in the static structure factor $S(k_{\max})$, and (3) the nonbonded potential energy density $\underline{E}_{\mathrm{NB}}$.

The remainder of the paper is nontraditionally organized. The simulation details are supplied in the Appendix. These are standard, commonly studied systems[2,14,15] with no novel or unusual simulation techniques applied. The body of this paper is composed of one section for each metric including motivation, definitions, calculation methods, and discussions of the results particular to that metric. The final two sections discuss the wider applicability of our findings and summarize our important results.

II. PACKING FRACTION

Free volume theories are the most common example of collapsing mobility data near the glass transition into a master curve. The central idea is that τ is a function only of the fraction of the volume that is ''occupied'' by atoms. When the volume is completely occupied, all mobility vanishes, or equivalently, the relaxation time is infinite.[16] There are three important facets of this approach. First, a plot of mobility vs occupied volume fraction will form a single curve regardless of the temperatures and pressures of the various experiments. Second, for any temperature and pressure, the occupied volume fraction can be used to define a distance to the point at which all mobility vanishes. Third, the point at which mobility vanishes is given a physical basis (space is full).

Intuitively, it is a simple matter to divide the volume into space occupied by atoms and void space. Characterizing the void volume distribution can be done for model systems

through successive particle insertion[17] by keeping statistics about the sizes successfully inserted in a simulation or by determining the work required to insert particles of various sizes through theory. Experimentally, one can use positron annihilation lifetime spectroscopy to determine average void volume.[18] These three methods all assume spherical cavities. Voroni tessellation identifies void volume distribution without requiring spherical cavities, but is primarily limited to simulated systems.[19] A more severe difficulty with characterizing the void volume distribution is that, frequently, the useful quantity is the ratio of total occupied space to the total space and is not the average size of a void or even simply the void size distribution.

The other alternative is to determine the occupied volume and then subtract this from the total volume to calculate void volume—a procedure that is not necessarily straightforward. The crux of the matter is what constitutes occupied volume? The Doolittle theory of free volume[3] defines the occupied volume through the density extrapolated to zero temperature (with no phase changes). This worked quite well for alkanes at atmospheric pressure.[3] However, it is not obvious that occupied volume is constant with temperature. It is quite common in polymer research to define occupied volume as the extrapolated zero-temperature volume but to allow for an increase in this volume with temperature via the coefficient of thermal expansion.[5,20] Neither of these methods includes the effect of pressure on occupied volume.

In the current study, the first scalar metric considered is based on the general free volume ideas. However, we use an atomistic approach to define occupied volume. In liquid state theory, it is common to use a reference system whose properties are easily defined and then to make modifications to approximate systems that are more complex.[21] One of the main premises of liquid state theory is that dense systems are governed mostly by the repulsive interactions.[22] Thus, it seems reasonable to map a dense system of interacting atoms to an equivalent system of hard spheres. A system of hard spheres can be divided unambiguously into occupied and free volume through the packing fraction.

The packing fraction η is a relative measure of the space filled by spheres to the total volume and is a gauge commonly used to quantify molecular structure in liquid state theory.[21] A packing fraction of $\eta=0.5$ indicates that half the volume is filled by the atoms whereas $\eta=0.74$ corresponds to a system composed of identical spheres in a close-packed lattice. For glassy systems, it is expected that the relaxation time would become infinite near the random close packed value[23] of $\eta=0.64$. Indeed, experimentally, colloids[24] have a dynamic transition at about $\eta=0.58$.

The packing fraction for a system of monodisperse hard spheres can be calculated[21] as

$$\eta=\frac{\pi}{6}d^3\rho, \tag{4}$$

where d is the sphere diameter and ρ is the number density of sites. To map our systems onto hard spheres, we need a means to calculate the effective hard sphere diameter d. We do this using the Barker-Henderson relation[25]

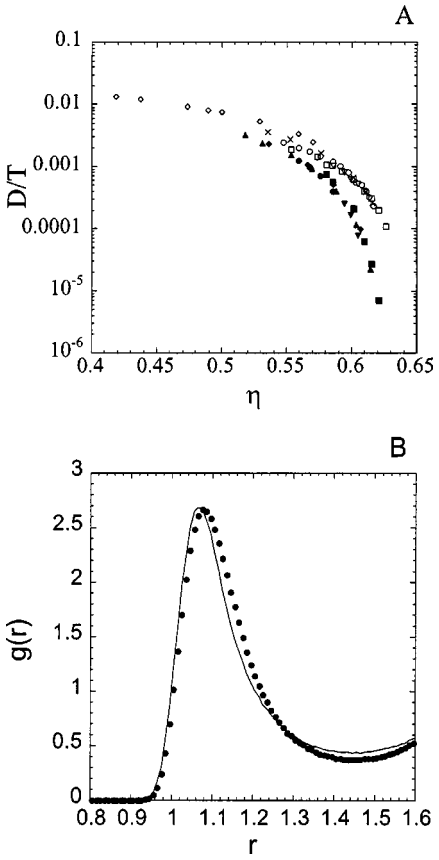

FIG. 3. (a) Repeat of Fig. 1(b) without using Eq. (6). (b) Pair correlation function for attractive (circles) and repulsive (line) systems at $T=0.50$, $\rho=1.06$.

$$d=\int_0^\infty\{1-\exp[-\beta U_{\mathrm{LJ}}^R(r)]\}dr, \tag{5}$$

where U_{LJ}^R is the potential from Eq. (A2) with $R_c=2^{1/6}\sigma$ and β is $1/T$. Figure 3(a) shows that simply using Eq. (5) for both the attractive and repulsive systems results in collapse to curves that are attraction dependent. The derivation of Eq. (5) included the substitution of the hard sphere pair correlation function for the system pair correlation function. While this approach works well for the repulsive systems, attractive systems need an additional correction.

Figure 3(b) shows the pair correlation function for an attractive system and a repulsive system at the same temperature and density. The position of the first peak in the attractive system is at a slightly larger distance than in the repulsive system. Though this difference may seem small, packing fraction is sensitive to small variations in hard sphere diameter. Thus, to correct for this minor difference and to achieve the collapse in Fig. 1(b), the attractive systems use Eq. (5) to calculate d^R for the repulsive system at the same temperature and density and then rescale d^R using

$$d=d^R\frac{r_{\mathrm{peak}}^A}{r_{\mathrm{peak}}^R}, \tag{6}$$

where r_{peak} is the location of the first peak in the pair correlation function and superscripts A and R refer to attractive and repulsive systems, respectively. Interpolations of the first

TABLE I. Comparison of fit values with other relevant quantities.

	Scalar metric		
Fit parameter	Packing fraction η	Nonbonded potential energy density E_{NB}	Static structure factor first peak values $S(k_{\max})$
Comparison value	0.64[a]	−6.9[c]	2.85[d]
$X_{\max}$	0.68[b]		3.85–4.10[e]
X_0 Eq. (11)	0.675	−6.1	4.0
X_c Eq. (12)	0.64	−5.75	3.5
γ	1.64	2.0	2.77

[a]Value from random close packing for hard spheres (Ref. 23).
[b]Value for maximally jammed ellipsoids (Ref. 26).
[c]Value found from a hcp crystal (Ref. 39) using Lennard-Jones interactions with neighbors out to the cutoff used in Eq. (A2).
[d]Value for a Lennard-Jones crystal (Ref. 30).
[e]Value for a Lennard-Jones glass from mode-coupling theory (Ref. 32).

peak locations were employed only if no repulsive system was run at the state point necessary for an attractive system.

The adoption of the packing fraction as the scalar metric leads to great simplification of the data in Fig. 1(a). For all temperatures and all pressures, for both isochors and isobars, for both attractive and repulsive interactions, all mobilities collapse to a single curve [Fig. 1(b)]. It can be seen that the effects of temperature, density, and potential interaction have been incorporated into the packing fraction. The fit divergences ($\eta_0=0.675$, $\eta_c=0.64$) are within the ranges for hard spheres in random close packed structures[23] ($\eta=0.64$) or ellipsoids in maximally jammed[26] states ($\eta=0.68$) as can be seen in Table I.

Packing fraction is commonly used to describe the glass transition in hard spheres[27] and colloids.[28] While it is standard practice to map other systems onto hard spheres to estimate many thermodynamic and transport properties,[21] it is less common to describe the state point of the systems in terms of packing fraction. We have previously used packing fraction in this same manner for a different system.[29]

To extend our method to more chemically detailed systems and experimental data, it may be more convenient to use a packing fraction defined as a ratio of densities to eliminate the necessity of defining an effective sphere. One could use as a reference point the high-pressure density found from an equation of state at a given temperature. The choice of reference state makes our method distinct from previous free volume theories. We expect the descriptive equation for mobility as a function of packing fraction defined in this manner to include a divergence as seen here. However, that divergence would not be restricted to values appropriate to hard spheres, it is probable that the maximum packing fraction would have values more appropriate to ellipsoids or cylinders and would be strongly system dependent.

III. STATIC STRUCTURE FACTOR

In principle, the static structure factor $S(k)$ provides information needed to calculate the packing fraction; however, the level of accuracy required to extract the site volume makes direct evaluation from $S(k)$ extremely difficult. Instead, we used the structure factor itself as the second scalar metric.

As the temperature is decreased, the most obvious change in $S(k)$ is that the height of its first peak grows. The height of the structure factor at the first maximum is a particularly intriguing choice for a metric. Previously, this height at the first maximum $S(k_{\max})$ has been used as a basis of theories of phase transitions. The Hansen-Verlet[30] criteria for crystallization is $S(k_{\max})\sim 2.85$ which works surprisingly well for a wide range of liquids.[31] More recently, $S(k_{\max})$ has been used as the primary input for mode-coupling theories of the glass transition.[7] This structure factor metric has the advantage over the packing fraction metric because it may be experimentally measured, although not straightforwardly. On the other hand, it lacks the clear physical picture associated with packing fraction.

One of the definitions of the static structure factor is[21]

$$S(k)=\frac{1}{N}\langle\rho_k\rho_{-k}\rangle, \tag{7}$$

where ρ_k is the number density at wave vector k, N is the number of sites, and the angle brackets denote an ensemble average. This quantity can be obtained through scattering experiments. It can also be obtained through the Fourier transform of the pair correlation function

$$S(k)=1+\rho h(k), \tag{8}$$

where k is the wave number (the system was assumed isotropic so angle dependence already has been integrated) and $h(r)$ is the total correlation function. The total correlation function is

$$h(r)=\frac{\langle n(r)\rangle_{\mathrm{actual}}}{\langle n(r)\rangle_{\mathrm{ideal}}}-1, \tag{9}$$

where $n(r)$ is the number of sites at a distance r from a given site and angle brackets denote averages over sites and configurations. The subscript ''actual'' refers to numbers calculated from simulation and ''ideal'' refers to the value from an ideal gas at the same site density. The calculation of $h(r)$ is done as a histogram with a small bin width (0.002σ).

One of the difficulties is that $h(r)$ can only be calculated for distances less than half a simulation box length. In the dense systems, this means that $h(r)$ has not yet decayed to the value of zero. In order to extend our $h(r)$ data to this range, the last few of peaks in $h(r)$ have been fit to the function

$$h^{\mathrm{extend}}(r)=A\exp(-\alpha r)\sin(Br), \tag{10}$$

where A, B, and α are adjustable parameters. This is merely an extrapolation tool so that $h(r)$ goes to zero in an oscillatory manner. However, with $h(r)$ now a function that becomes identically zero, it can be Fourier transformed into $S(k)$. There are still some minor problems with very small k since applying this ''tail correction'' is not exact, but the main peak in $S(k)$ is unaffected by this extrapolation.

In Fig. 1(c) $S(k_{\max})$ is shown to produce a master curve similar to that of the packing fraction, although with somewhat more scatter. Most scatter arises from errors in extract-

ing the structure factor from the simulations. The divergences ($S_c=3.5$, $S_0=4.0$) occur at values similar to values from mode-coupling theory found for Lennard-Jones fluids[32] ($S_{\max}=3.85-4.1$) (see Table I). One drawback to using the static structure factor as a metric may be its lack of sensitivity to molecular potential details. Several previous studies have shown that the specific potential chosen can have a marked effect on the dynamics of a system yet with no effect on the structure factor.[33] For example, in simulations of polybutadiene, turning off the torsions did very little to the static structure factor.[33–35] However, the relaxation functions decayed much faster without the torsions.[34] The mean square displacement of the methylene groups changed from a ''caged'' behavior to one with no plateau upon turning off the torsions.[34,35] While this argues against the idea of a universal value for $S(k_{\max})$ that defines the glass transition, it need not invalidate the concept that the first peak collapses all mobility data *for a given system*. This hypothesis should be tested further on systems with multiple length scales.

An additional complication stems from the difficulties involved in extracting the static structure factor from experiments. Unfortunately, while $S(k)$ can be obtained from scattering experiments, the details can be difficult to extract due to the nature of the experimental compromises that must be made between range, intensity, and energy.[36] In our simulations, there is a change in $S(k_{\max})$ along both isochors and isobars. Neutron scattering experiments on orthoterphenyl[37] and polybutadiene[38] are reported to show no change in $S(k)$ along isochors, but a substantial change along isobars and isotherms. Nonetheless, changes in the system dynamics are observed along all three thermodynamic paths. To extract $S(k)$ from experiments, it is common to use fitting functions on the intensity data. Since these experimental data were fit by matching peak position and width, it is unclear whether the heights have been adequately captured. Our peak positions and widths are constant along an isochor; it is the height that changes as shown in Fig. 4.

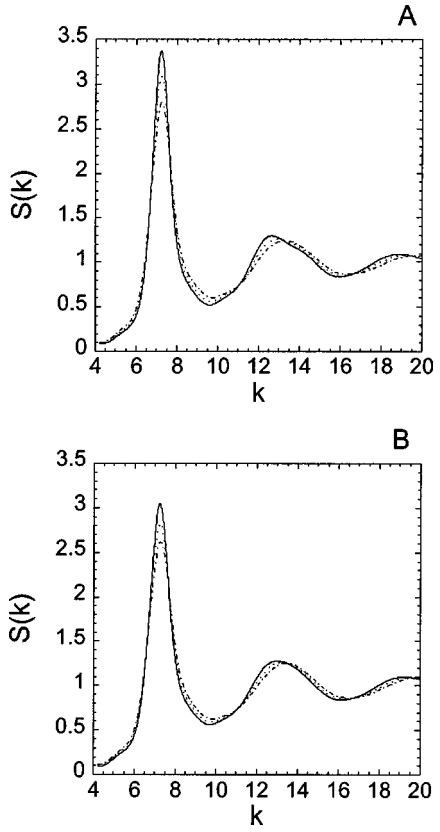

FIG. 4. $S(k)$ as a function of temperature at a $\rho=1.06$. Solid line $T=0.50$, dotted line $T=0.70$, dot-dashed line $T=1.0$ (a) attractive systems (b) repulsive systems.

IV. NONBONDED ENERGY DENSITY

The selection of the above metrics focused on the repulsive portion of the interactions; both the structure factor and the packing fraction are insensitive to the attractive portion of the assumed interactions. Our third metric, the nonbonded potential energy density, focuses primarily on the attractions. Here, lower values of this energy correspond to more dense packing configurations that, again, could lead to reduced mobility.

The nonbonded potential energy density is calculated straightforwardly as the average LJ energy per site (excluding the 1–2 bonded neighbors) multiplied by the number density. The average is taken over both sites and time steps. This is, of course, only valid for the attractive systems. Due to the short range of the interaction in the repulsive systems, the nonbonded potential energy density is not a useful metric in that case.

For the attractive systems, however, the nonbonded energy density also generates a master curve as shown in Fig. 1(d). As seen in Table I, the divergence occurs near a value of -6 ($\underline{E}_{\mathrm{NBc}}=-5.75$, $\underline{E}_{\mathrm{NB0}}=-6.1$). Interestingly, the minimum nonbonded potential energy density for a system of unconnected, monodisperse Lennard-Jones spheres occurs at hexagonal close packing (hcp) (Ref. 39) with a value of -6.9 (in Lennard-Jones units). The chain nature of our simulation would increase this value slightly. Therefore, it seems that the glass transition occurs near the minimum nonbonded potential energy density available to the system.

This point is examined more carefully in Fig. 5. Here, the nonbonded energy (not the energy density) is plotted as a function of temperature for three simulations series at different densities: $\rho=1.0$, 1.033, and 1.06. A reduced density of 1.0 implies that one site fits exactly into a cube with side

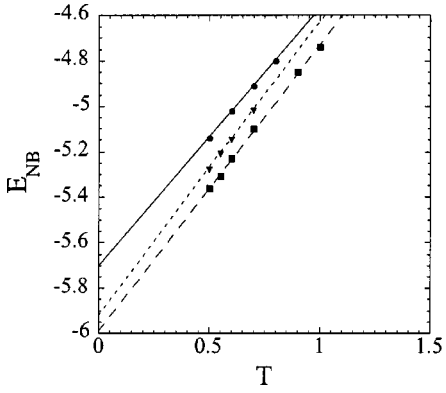

FIG. 5. Nonbonded energy vs temperature for attractive systems at $\rho=1.00$, 1.033, and 1.06 with same symbols as in Fig. 1.

length of σ. Coincidentally, this corresponds to the density of a unit cell for a Lennard-Jones hcp system. Using the critical nonbonded energy density of -5.75 from the power law fit, the corresponding values of the critical nonbonded energy are -5.75, -5.57, and -5.42, respectively. It can be seen from Fig. 5 that the density of 1.0 hits its critical nonbonded energy value at a temperature of zero. The higher densities will achieve their critical nonbonded energy values at higher temperatures. This implies that the density must be greater than some value to form a glass. This has been noted previously in the literature for a different system.[40] Thus, it is entirely possible that isochors will not show the same behavior as isobars if the density is not above this threshold value. Indeed, for isobars that are too far from this threshold value, the behavior may not fall on the master curve. In fact, if the VF fit value is used, the density of 1.0 will not achieve the necessary nonbonded energy at positive temperature.

While not applicable to repulsive systems, the nonbonded potential energy density has several strong points. First, it is easily calculated from simulations for any attractive system regardless of the fidelity of the model. Second, it can be approximately extracted from experimental data as described for viscoelastic systems in Ref. 41. Third, this metric, embedded within a nonlinear viscoelastic formalism, was able to predict accurately the range of behaviors seen in glassy polymers ranging from enthalpy relaxation to physical aging to mechanical yield.[42]

V. DISCUSSION

In the previous three sections, we have discussed the particulars of the three scalar metrics of packing fraction, first peak value in static structure factor, and nonbonded energy density. Here, we discuss the commonalities and connections among the three metrics. The master curves using all three metrics X could be reasonably fit with either the Vogel-Fulcher equation (Fig. 1)

$$\ln\left(\frac{D}{T}\right)=A+\frac{B}{X-X_0}, \tag{11}$$

where A, B, and X_0 are system dependent constants or with the critical phenomena power law form (Fig. 6)

$$\frac{D}{T}\propto|X-X_c|^{\gamma}, \tag{12}$$

where X_c is the critical value of the scalar metric and γ is the critical exponent. The parameters from these fits are given in Table I. The power law divergence X_c always occurs before the VF divergence X_0. However, both values seem reasonable when compared to estimates for similar systems using different methods. Packing fraction has a divergence near the value given for hard spheres. The nonbonded potential energy density is higher (i.e., less negative) than that of a LJ crystal, but not absurdly so. The static structure factor first peak value is similar to values found for crystallization of a LJ system and for mode-coupling theory values of a LJ glass. The critical exponent γ should indicate the class of transition. As seen in Table I, γ values for these three scalar metrics are within the reasonable range of 1–3.

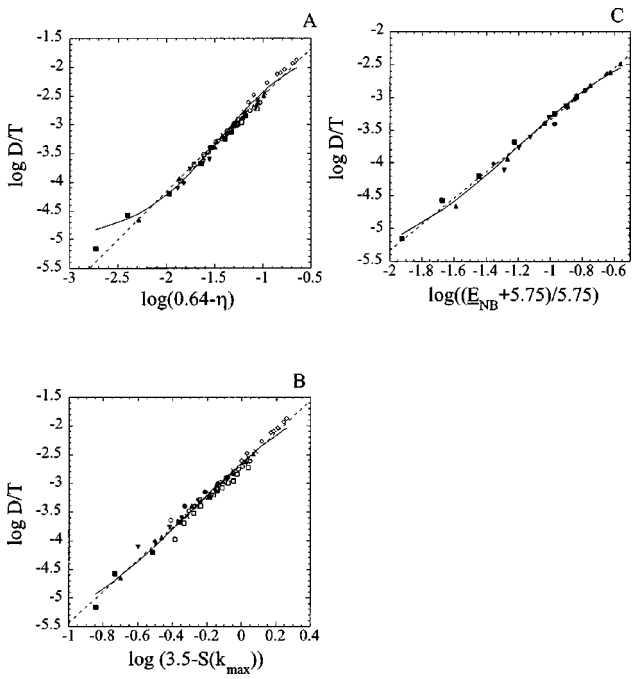

FIG. 6. Comparing the fit of Eqs. (11) (solid line VF fit) and (12) (dashed line power law fit) for D/T using all three scalar metrics. Symbols are the same as in Fig. 1. (a) mobility as a function of η (b) mobility as a function of $S(k_{\max})$ (c) mobility as a function of E_{NB}.

As one might expect, the three scalar metrics (packing fraction, nonbonded energy density, and first peak value in static structure factor) are correlated. Figure 7 shows first peak value of the static structure factor as a function of packing fraction and of nonbonded energy density. There are some general trends. High density and low temperature are associated with higher first peak values, higher packing fractions, and nonbonded energy densities that are more negative.

It is not clear that any of these quantities can be interpreted as the sole cause of mobility or even that any of the three is the most fundamental quantity. It is clear that all three are correlated with mobility and can be used to collapse data into master curves. We have shown that relations incorporating a divergence in the mobility can be used to fit the data. Moreover, these fits have physically reasonable values for the scalar metric at the divergence point.

VI. CONCLUSIONS

While it is a common practice to correlate mobility as a function of temperature, this is a strongly path dependent correlation due to the effects of density. One way to circumvent the difficulties of the relative contributions of temperature and density is to select parameters that are functions of both temperature and density, but perhaps not simple functions. We have done that through our scalar metrics of packing fraction, first peak value of the static structure factor, and nonbonded energy density.

Packing fraction, to some extent, ameliorates one of the common flaws in free volume since it simply gives an overall average and does not specify average void sizes or distributions. Packing fraction incorporates temperature and den-

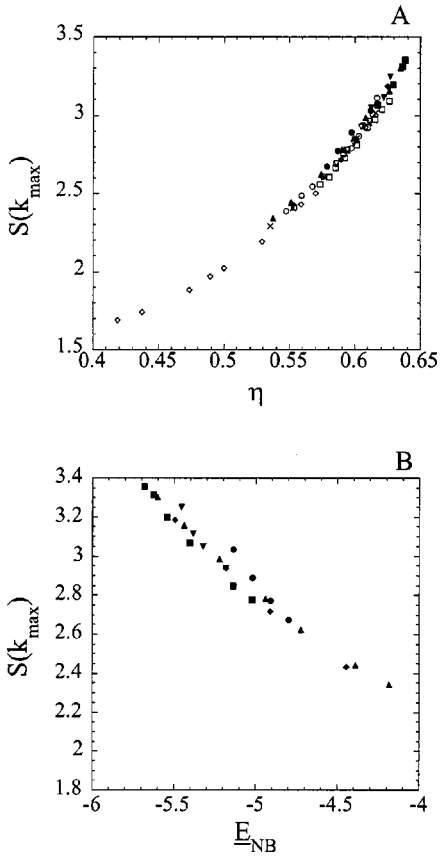

FIG. 7. $S(k_{\max})$ as a function of (a) η and (b) E_{NB}. Symbols are the same as Fig. 1.

sity effects by using a reference state of hard spheres, which change size as a function of P-V-T properties. By choosing an appropriate reference state, it may be possible to generalize the benefits of packing fraction to more chemically detailed systems. However, if we take the view that there is a continuum of systems from purely temperature dominated to purely density dominated, packing fraction may have less universal applicability than one would hope.

The first peak value of the static structure is available from experiment, simulation, and theory. The main difficulty with it is that the divergence value is not guaranteed to be a universal value as is frequently assumed for mode-coupling theory. The Hansen-Verlet rule and naive mode-coupling theory both assume a single relevant length scale. Increasing the complexity of a system frequently adds more length scales. These multiple length scales will influence the static structure factor. In addition, the experimental difficulties in determining the peak values may also hinder use of this scalar metric.

Nonbonded potential energy density is clearly not the correct choice for systems in which attractive potential energy is not a major contribution. While our attractive system data have shown collapse to a single master curve, it is entirely possible that nonbonded energy density would need to change to specific potential energy to include more complicated interactions for realistic systems. Preliminary results on an experimental system show very good results in aging predictions by scaling relaxation times with specific potential energy even below the glass transition.[42]

In this study, we have performed molecular dynamics simulations of penetrant-chain systems with the purpose of correlating mobility with static properties. This method incorporates both density and temperature effects using scalar metrics. We found that we could create master curves of mobility using as scalar metrics: packing fraction, first peak value of the static structure factor, and nonbonded energy density.

APPENDIX: SYSTEM SPECIFICATIONS

The systems under study are based on the Kremer-Grest model.[15] The bonding potential U_{bond} is

$$U_{\mathrm{bond}}(r) = -0.5HR_0^2 \ln\left[1-\left(\frac{r}{R_0}\right)^2\right] \quad r<R_0$$

$$U_{\mathrm{bond}}(r) = \infty \quad \text{otherwise}, \tag{A1}$$

where H is set to 30 and R_0 is equal to 1.5. In addition, sites have a Lennard-Jones potential applied to them

$$U_{\mathrm{LJ}}(r) = 4\epsilon\left[\left(\frac{\sigma}{r}\right)^{12}-\left(\frac{\sigma}{r}\right)^{6}\right]+U_0 \quad r<R_c,$$

$$U_{\mathrm{LJ}}(r) = 0 \quad r>R_c, \tag{A2}$$

where ϵ and σ are both set to unity, U_0 is the value needed to make $U_{\mathrm{LJ}}(R_c)=0$, and R_c is a cutoff radius. All sites directly bonded to each other have $R_c=2^{1/6}\sigma$. Systems were run with two different cutoffs used for the nonbonded interactions (this includes 1–3 and 1–4 neighbors). Repulsive systems were run with $R_c=2^{1/6}\sigma$ also, while attractive systems were run with $R_c=2\times 2^{1/6}\sigma$.

All systems were 80 chains (with ten sites each) and five single sites. Penetrants had the same LJ interactions as the nonbonded chain sites. Molecular dynamics simulations were performed using the LAMMPS code.[43] A velocity Verlet algorithm with Nosé-Hoover thermostat was used. The time step was 0.002 (in LJ units) and the friction constant was set to a value based on energy fluctuations at each state point. All production runs used NVT conditions and a number of production runs were done for each state point with the reported values as averages of runs at the same state point. NPT simulations were done solely to obtain a density at a given temperature and pressure. Systems were considered equilibrated when three conditions were met. First, the various thermodynamic quantities (temperature, energy components, and pressure) were stable. Second, the mean square displacement (MSD) of the chain center of mass was greater than the squared radius of gyration. Third, the normalized second Legendre polynomial of the end-to-end vector had decayed to less than 0.1. These are necessary conditions for equilibration although they are not sufficient. State points that required more than 100 million time steps to reach these conditions were discarded in the analysis.

Diffusion coefficients for chain centers of mass were calculated from

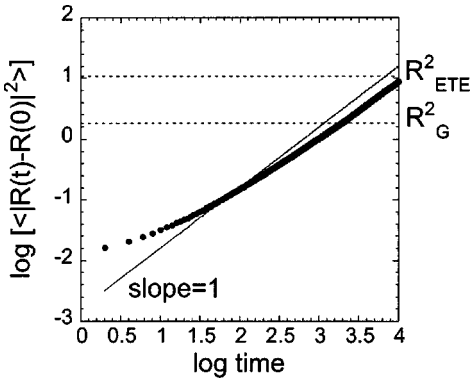

FIG. 8. Mean-square displacement versus time. Symbols are simulated data for chain center of mass $T=0.7$ rho$=1.06$ attractive system. Solid line is a slope of 1. The dotted horizontal lines denote the radius of gyration (lower line) and end-to-end distance (upper line).

$$D=\frac{1}{6}\frac{d\langle|\vec{R}(t)-\vec{R}(0)|^2\rangle}{dt}, \tag{A3}$$

where $\vec{R}(t)$ is position at time t and the angle brackets denote average over all chains and multiple time origins. This is equivalent to the Einstein relation at long times. The data region fit corresponds to the region where ln(MSD)-ln t has a slope of unity. An example of this log-log plot is shown in Fig. 8. The chain center-of-mass mean-square displacement has a slope of unity at long times. Also on that plot are values for the radius of gyration and the end-to-end distance. The figure shows equilibrating for movement greater than a radius of gyration and restarting the simulation for several production runs should result in significant overall motion in the system.

[1] This can be seen later in our paper for parameters other than temperature in Fig. 6.
[2] C. Bennemann, W. Paul, K. Binder, and B. Dünweg, Phys. Rev. E **57**, 843 (1998).
[3] A. K. Doolittle, J. Appl. Phys. **22**, 1471 (1951).
[4] M. H. Cohen and G. S. Grest, Phys. Rev. B **20**, 1077 (1979).
[5] R. Simha and R. F. Boyer, J. Chem. Phys. **37**, 1003 (1962).
[6] J. H. Gibbs and E. A. DiMarzio, J. Chem. Phys. **28**, 373 (1958).
[7] U. Balucani and M. Zoppi, *Dynamics of the Liquid State* (Oxford University Press, Oxford, 1994).
[8] Y. J. Jung, J. P. Garrahan, and D. Chandler, cond-mat/0311396.
[9] G. Tarjus, D. Kivelson, S. Mossa, and C. Alba-Simionesco, J. Chem. Phys. **120**, 6135 (2004).
[10] C. M. Roland, R. Casalini, P. Santangelo, M. Sekula, J. Ziolo, and M. Paluch, Macromolecules **36**, 4954 (2003).
[11] C. M. Roland and R. Casalini, Macromolecules **36**, 1361 (2003).
[12] R. Casalini and C. M. Roland, cond-mat/0403622.
[13] An equation of state developed several years ago suggested that the relevant corresponding state variables could be related to van der Waals volume, fractional free volume, and cohesive energy density. I. C. Sanchez and J. Cho, Polymer **36**, 2929 (1995).
[14] C. Bennemann, W. Paul, J. Baschnagel, and K. Binder, J. Phys.: Condens. Matter **11**, 2179 (1999).
[15] G. S. Grest and K. Kremer, Phys. Rev. A **33**, 3628 (1986); K. Kremer and G. S. Grest, Phys. Rev. Lett. **61**, 566 (1988); K. Kremer and G. S. Grest, J. Chem. Phys. **92**, 5057 (1990).
[16] The first instance of a free volume argument dates from about 400 BC when Democritus concluded that because there is motion in the world that matter must contain both occupied and free volume which he called ''atoms and the void.'' See p. 103, K. Popper, *The World of Parmenides* (Routledge, NY, 1998).
[17] J. Budzien, J. D. McCoy, D. Rottach, and J. G. Curro, Polymer **45**, 3923 (2004).
[18] J. Bartos and J. Kristiak, J. Phys.: Condens. Matter **11**, A371 (1999).
[19] F. W. Starr, S. Sastry, J. F. Douglas, and S. C. Glotzer, Phys. Rev. Lett. **89**, 125501 (2002).
[20] T. G. Fox and P. J. Flory, J. Appl. Phys. **21**, 581 (1950); T. G. Fox and P. J. Flory, J. Polym. Sci. **14**, 315 (1954).
[21] J. P. Hansen and I. R. McDonald, *Theory of Simple Liquids*, 2nd ed. (Academic, London, 1990).
[22] J. D. Weeks, D. Chandler, and H. C. Andersen, J. Chem. Phys. **54**, 5237 (1971).
[23] J. D. Bernal and J. Mason, Nature (London) **188**, 910 (1960).
[24] E. R. Weeks, J. C. Crocker, A. C. Levitt, A. Schofield, and D. A. Weitz, Science **287**, 627 (2000).
[25] J. A. Barker and D. Henderson, J. Chem. Phys. **47**, 4714 (1967).
[26] A. Donev, I. Cisse, D. Sachs, E. A. Variano, F. H. Stillinger, R. Connelly, S. Torquato, and P. M. Chaikin, Science **303**, 990 (2004).
[27] R. J. Speedy, Mol. Phys. **95**, 169 (1998).
[28] G. Foffi, G. D. McCullagh, A. Lawlor *et al.*, Phys. Rev. E **65**, 031407 (2002).
[29] J. Budzien, J. D. McCoy, and D. B. Adolf, J. Chem. Phys. **119**, 9269 (2003).
[30] J.-P. Hansen and L. Verlet, Phys. Rev. **184**(1), 151 (1969).
[31] S. W. Rick, J. D. McCoy, and A. D. J. Haymet, J. Chem. Phys. **92**, 3040 (1990).
[32] U. Bengtzelius, Phys. Rev. A **33**, 3433 (1986).
[33] S. Kruchev, W. Paul, and G. D. Smith, Macromolecules **35**, 4198 (2002).
[34] S. Krusev and W. Paul, Phys. Rev. E **67**, 021806 (2003).
[35] W. Paul, Polymer **45**, 3901 (2004).
[36] J. S. Higgins and H. C. Benoît, *Polymers and Neutron Scattering* (Clarendon, Oxford, 1994).
[37] A. Tölle, Rep. Prog. Phys. **64**, 1473 (2001).
[38] B. Frick, C. Alba-Simionesco, K. H. Andersen, and L. Willner, Phys. Rev. E **67**, 051801 (2003).
[39] The lowest energy crystal for a Lennard-Jones system is hcp not fcc. See J. O. Hirschfelder, C. F. Curtiss, and R. B. Bird, *Molecular Theory of Gases and Liquids* (Wiley, New York, 1954), p. 1041.
[40] S. Sastry, Phys. Rev. Lett. **85**, 590 (2000).
[41] D. B. Adolf, R. S. Chambers, and J. M. Caruthers, Polymer **45**, 4577 (2004).
[42] D. B. Adolf, R. S. Chambers, and J. M. Caruthers, Polymer **45**, 4599 (2004).
[43] LAMMPS version 4.0 licensed from Sandia National Laboratories; S. J. Plimpton, J. Comput. Phys. **117**, 1 (1995).